Excited states in ^{139}Sm described with the interacting boson model plus broken pairs

C. Rossi Alvarez,[1] D. Vretenar,[2] Zs. Podolyák,[1,*] D. Bazzacco,[1] G. Bonsignori,[3] F. Brandolini,[1] S. Brant,[2] G. de Angelis,[4] M. De Poli,[4] M. Ionescu-Bujor,[5] Y. Li,[4,†] S. Lunardi,[1] N. H. Medina,[1,‡] and C. M. Petrache[1,5]

[1]*Dipartimento di Fisica dell'Università and INFN, Sezione di Padova, Padova, Italy*

[2]*Physics Department, Faculty of Science, University of Zagreb, Zagreb, Croatia*

[3]*Dipartimento di Fisica dell'Università and INFN, Sezione di Bologna, Bologna, Italy*

[4]*INFN, Laboratori Nazionali di Legnaro, Legnaro, Italy*

[5]*Institute of Physics and Nuclear Engineering, Bucharest, Romania*

(Received 12 February 1996)

The high-spin structure of ^{139}Sm has been studied through the ^{110}Pd(^{34}S,5n) reaction at beam energies of 150 and 165 MeV. The level scheme has been extended up to an excitation energy of 11.1 MeV and spin $61/2^+$. A band built on the $\nu i_{13/2}$ $[660]1/2^+$ intruder orbital has been established and firmly linked to the known lower-spin levels in the nucleus. The low-lying states of both parities as well as a relatively strong $\Delta I=1$ regular structure observed above spin $27/2^-$ are nicely reproduced by the interacting boson-fermion model with broken pairs. [S0556-2813(96)00707-8]

PACS number(s): 23.20.Lv, 21.60.Fw, 25.70.Gh, 27.60.+j

I. INTRODUCTION

The nuclei lying in regions of transition between spherical and well-deformed shapes have always been recognized as an excellent testing ground for various nuclear models. In general, nuclear models have been developed for describing the level structure of either spherical or well-deformed nuclei and therefore, if they happen to also reproduce the structure of the transitional ones, they are considered to be of more fundamental validity. The high-spin excitation states of deformed medium heavy nuclei have often been successfully explained by the deformed cranked shell model (CSM) [1]. In particular, the existence of superdeformed (SD) shapes in the almost ''spherical'' nuclei of the transitional region with $A\approx 140$, like ^{143}Eu and ^{144}Gd, was predicted by the CSM [2], and later on confirmed experimentally [3,4]. Moreover, highly deformed (HD) intruder bands have been found to coexist, at high spin, with the states of normal deformation in some odd-even nuclei of this same region [5]. These bands are interpreted as being built on the neutron $i_{13/2}$ orbital which intrudes from the $N=6$ oscillator shell, and, at large deformations, approaches the Fermi surface. Here, we consider as normal deformed bands or states based on orbitals with $N=4$ or 5.

The shape of transitional $A\simeq 140$ nuclei below the $N=82$ shell closure is characterized by a small quadrupole deformation $\beta_2=0.1-0.2$, and concepts like triaxiality and/or γ softness have been often introduced in order to reproduce experimental data. However, the low-spin structure appears more ''spherical-like'' and cannot be accounted for by the cranking approximation. Therefore, in order to describe their level structure at normal deformation, other nuclear models have to be used.

Among these, the interacting boson-fermion model [6], which provides a consistent description of low-spin nuclear structure from the spherical [SU(5)], to the rotational [SU(3)] limit has been one of the most successful. The IBM-IBFM model is also particularly interesting because it is able to describe the physics of high-spin states [7] if, in addition to bosons, selective noncollective fermion pair states are included in the model space through the successive breaking of the correlated S and D pairs (s and d bosons). This extension of the model is especially relevant for transitional regions, where single-particle excitations and vibrational collectivity are dominant modes and no clear axis for cranking exists. For odd-A nuclei [8], the IBFM plus broken pairs describes one- and three-fermion states.

In the present paper we report a detailed study of the low- and high-spin level structure of the $N=77$ nucleus ^{139}Sm performed with the γ-detector array GASP. The present work extends a previous study done some years ago at Legnaro using a smaller array of Ge detectors [9]. Among the various structures observed in ^{139}Sm, a $\nu i_{13/2}$ intruder band has been clearly identified and firmly connected to the lower-spin states. We mention here that three transitions of the $\nu i_{13/2}$ band were already seen in our previous study [9], even if not recognized as members of a collective band. In a recent parallel work performed at Stony Brook [10] the same band was observed, but it has been connected to the normal-deformed states in a way which is not confirmed by our data. Preliminary results on the decay-out of this HD band have been published in conference proceedings [11]. In order to characterize the deformation of the intruder band we have also undertaken a Doppler shift attenuation method lifetime analysis, which gives a quadrupole moment smaller than that of similar bands in neighboring nuclei [12–14].

Calculations performed in the framework of the interacting boson-fermion model plus broken pairs reproduce in de-

*On leave from Institute of Nuclear Research of the Hungarian Academy of Sciences, Debrecen, Hungary.

†On leave from Institute of Physics, Academia Sinica, Shanghai, China.

‡Permanent address: Departamento de Fisica Nuclear, University of Sao Paulo, Sao Paulo, Brazil.

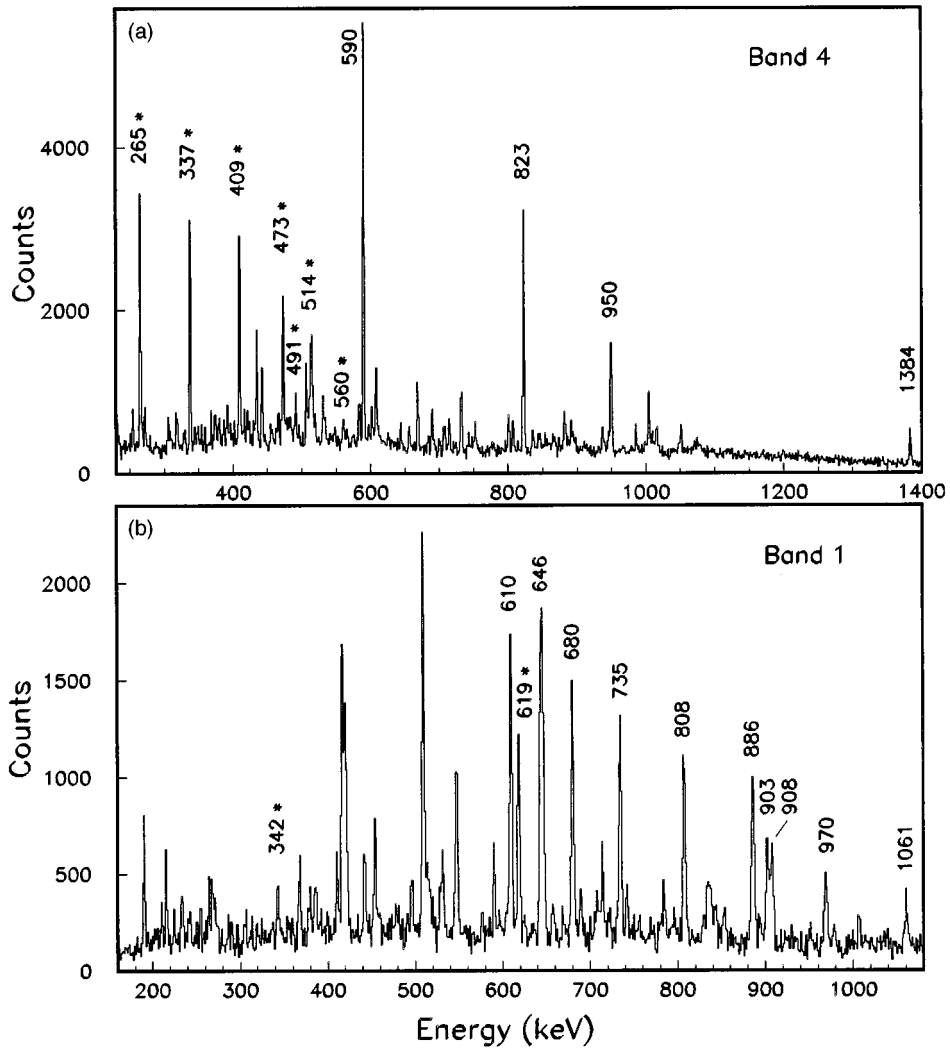

FIG. 1. (a) Double-gated coincidence spectrum for band 4, with gates set on all dipole transitions above spin $27/2^-$. The $\Delta I=1$ transitions are indicated by an asterisk. The data are from the thick-target experiment. (b) Double-gated coincidence spectrum with gates set on clean transitions of the $\nu i_{13/2}$ intruder band with energies higher than 650 keV. In-band transitions are labeled with their energies in keV and the two linking transitions of 618.5 and 342.3 keV are indicated additionally by an asterisk. The data are from the thin-target experiment.

tail the structure of states with normal deformation of both positive and negative parity up to spin 41/2.

II. MEASUREMENTS AND RESULTS

The ^{139}Sm nucleus has been populated through the ^{110}Pd(^{34}S,5n) reaction at beam energies of 150 and 165 MeV. The beam was delivered by the Tandem XTU accelerator of Legnaro National Laboratories and γ rays have been detected using the GASP array [15] composed of 40 Compton-suppressed high-efficiency HPGe detectors and an inner BGO ball of 80 crystals. Events have been collected on tape when at least three Compton-suppressed Ge detectors and three BGO detectors fired in coincidence.

In the experiment at 150 MeV of beam energy, the target consisted of two self-supporting foils of isotopically enriched ^{110}Pd for a total thickness of 1.1 mg/cm^2. In the one at 165 MeV, the target consisted of 0.9 mg/cm^2 of ^{110}Pd evaporated on a 15.6 mg/cm^2 gold backing. Typical beam intensities were around 5 pnA, giving a singles rate of $\approx$10 kHz in the individual Ge detectors and an event rate of $\approx$ 6 kHz. A total of 800 million triple- and higher-fold events has been collected in each experiment. We have to mention here that the experiment at 150 MeV had the main goal of studying the nucleus ^{140}Sm and therefore the chosen beam energy was not optimal for the population of ^{139}Sm. The data were helpful anyway for the study of the high-spin structure of ^{139}Sm, especially for the discovery of the $i_{13/2}$ intruder band.

Energy calibration of the spectra and gain matching between the different Ge detectors have been performed using standard γ-ray sources as well as known γ-ray transitions of ^{139}Sm and of the neighboring nuclei populated in the same reaction. The data have been sorted into fully symmetrized matrices and cubes with proper conditions on the fold and on the sum energy of the BGO ball. In order to enhance the different band structures seen in ^{139}Sm we made use of the triples data by constructing γ-γ matrices in coincidence with the strongest transitions in each observed regular sequence. Examples of doubly gated spectra showing two of the high-spin structures in ^{139}Sm are given in Fig. 1.

The spins and parities of the levels have been deduced

from the analysis of the directional correlation ratios from oriented states (DCO) for the ^{139}Sm transitions. A DCO γ-γ matrix has been created sorting on one axis the detectors lying at 90° with respect to the beam direction and on the other those at 34° and 146°. In the GASP geometry, if one gates on a stretched quadrupole transition, the theoretical DCO ratios $I_{90°}(\gamma)/I_{34°}(\gamma)$ are ≈ 1 for stretched quadrupole transitions and ≈ 0.5 for pure dipole ones. If, on the contrary, gates are set on a pure dipole transition, the expected DCO ratios for quadrupole and dipole transitions are ≈ 2 and ≈ 1, respectively.

The angular distribution results of our previous experiment performed at the small MIPAD [9] array were also used for determining the multipolarity of the strongest transitions. In that experiment, the ^{139}Sm nucleus was populated with the ^{114}Cd(^{29}Si,4n) reaction at a beam energy of 128 MeV and the γ-ray intensities have been measured at five different angles between 90° and 150°.

The γ-ray energies and relative intensities of the γ transitions belonging to ^{139}Sm, together with the DCO ratios, A_2 and A_4 angular distribution coefficients and spin-parity assignments are reported in Table I. The relative intensities were determined from the thick target experiment and normalized to the 590.0 keV $15/2^- \rightarrow 11/2^-$ transition.

III. THE LEVEL SCHEME OF ^{139}Sm

The level scheme of the ^{139}Sm nucleus deduced from the present study is shown in Fig. 2, where the excited states above ≈ 2.5 MeV are grouped in six different structures labeled from 1 to 6. The scheme is built above the few low-spin states known from β-decay studies [16]. The transitions have been placed in the level scheme on the basis of coincidence relationships and relative intensities. Spin assignments are based on DCO analysis, angular distribution results, and on decay patterns.

The parity of the levels has been established assuming that, when gating on a $\Delta I=2$ stretched quadrupole transition, the strong transitions with DCO ratios $\approx$ 1 have $E2$ character and the transitions with DCO ratios definitely different from 1 and 0.5 are of mixed multipolarity ($M1+E2$ character).

We confirm all the known levels below the $T_{1/2}=10.7$ s $11/2^-$ isomer at 457 keV and also the levels populated in the β decay of the nucleus ^{139}Eu lying at 589 and 721 keV. The spin proposed on the basis of logft values [16], are $I^\pi = 9/2^-$, $11/2^-$, $13/2^-$ for the 589 keV state and $7/2^+$ for the 721 keV state. Our angular distribution and DCO-ratio results for the 132.4 keV transition favor $I^\pi = 9/2^-$ or $13/2^-$ for the 589 keV state whereas those for the 453.8 keV transition are typical for a $\Delta I=1$ transition with $M1+E2$ character and therefore consistent with the proposed spin $7/2^+$ for the 721 keV state. We prefer the $9/2^-$ assignment for the 589 keV level on the basis of the available systematics in this mass region [17]. Such spins, together with those previously determined for the lower-lying levels [16], will serve as the basis for the spin-parity assignment of the higher-lying levels in ^{139}Sm.

Some of the spin assignments in the level scheme of Fig. 2 are different from those of the previous Padova-Legnaro study [9] and also from those of the parallel work of the Stony Brook group [10]. The DCO ratio for the 807.5 keV transition depopulating the level at 1074 keV is in fact not compatible with the previously proposed $\Delta I=1$ $E1$ character but instead, as is the case also for the above lying transitions of 379.7, 514.0, and 689.5 keV, is characteristic of a $\Delta I=2$ stretched $E2$ transition. This fixes the spin $21/2^+$ for the state at 2656 keV. The same spin assignment is obtained for this level if one considers the DCO ratios of the γ rays in the parallel sequence built above the $7/2^+$ level at 721 keV (416.5, 643.7, 509.3, and 368.0 keV). In the work of Vaska *et al.* [10], mainly from analogy with the neighboring nuclei, a spin $7/2^-$ was assigned to the state at 1137 keV and the 643.7 and 509.3 keV transitions were assumed to be of stretched $E2$ character. The DCO ratios for the 547.4 and 416.5 keV transitions can also lead to a $7/2^-$ assignment for the 1137 keV level but, from the DCO ratios of the upper transitions (especially the 509.3 keV one) it is not possible to get again for the level at 2656 keV the same spin $21/2^+$ as obtained from the previously discussed parallel cascade. Of course, it is always possible that one of the transitions which is assigned to be of $\Delta I=2$ $E2$ character is instead of $\Delta I=0$ character, since in both cases the same DCO ratio is obtained. This possibility has been carefully checked but excluded, since no solutions are found which are compatible with all the observed transitions and their measured DCO ratios.

The new spins proposed here for the lower-lying levels in ^{139}Sm modify, as a consequence, the spins proposed for the highly deformed band (which is labeled 1 in Fig. 2) in Ref. [10]. Moreover, our data show that the 609.5 keV γ ray, considered a linking transition in Ref. [10], is a member of the HD band, whereas it is the 618.5 keV transition which links it to the normal-deformed states carrying out 85% of the band intensity. In the spectrum of Fig. 1(b), in fact, the 618.5 keV γ ray exhibits an intensity smaller than that of the 609.5 keV in-band transition, thus showing its character of linking transition. The missing 15% intensity is carried out by the 342.3 keV transition which connects the lowest state of the band to the $19/2^+$ level at 2565 keV. The DCO ratio of the 618.5 keV linking transition indicates a stretched $E2$ character and fixes the spin $21/2^+$ for the lowest member of the HD band.

The high-spin part of the HD band has been established using the data of the thin-target experiment. The band has been extended up to 11.1 MeV excitation energy and spin $61/2^+$. The transition with $E_\gamma=1122$ keV placed on top of the band in Ref. [10] is not confirmed by our data. We observe instead in coincidence with the high-lying transitions of the HD band a 1120.7 keV transition which is part of a parallel cascade connecting the HD band to the 31/2 state of the structure labeled 3 in Fig. 2.

The angular distributions and DCO ratios for the strong transitions of the part of the level scheme built on the $11/2^-$ isomer allowed to unambiguously establish the parity of the states. The proposed positive parity for the state at 2197 keV is mainly based on the systematics of the $N=77$ isotones from ^{131}Xe to ^{137}Nd, where a $19/2^+$ isomeric state is observed to deexcite through a strong $E1$ transition to the $17/2^-$ level of the band structure built on the $11/2^-$ β-decaying level [18–21]. The lifetime of the $19/2^+$ state decreases systematically from 14 ns in ^{131}Xe to a few ns in

TABLE I. Energies, relative intensities, and DCO ratios of γ transitions assigned to ^{139}Sm from the ^{110}Pd + ^{34}S reaction at 165 MeV. The γ-ray angular distribution coefficients were determined from the ^{114}Cd(^{29}Si,$4n$)^{139}Sm reaction at 128 MeV beam energy.

E_γ (keV)	I_γ [a]	DCO [b]	A_2	A_4	$J_i^\pi \rightarrow J_f^\pi$	E_x (keV)
43.6	c				$5/2^+ \rightarrow 3/2^+$	267
72.2	60(12) [d]				$25/2^- \rightarrow 23/2^-$	3325
91.0	8(3) [d]				$21/2^+ \rightarrow 19/2^+$	2656
108.2	20(6) [d]		e		$21/2^+ \rightarrow 19/2^+$	2656
108.3	39(12) [d]		e		$13/2^+ \rightarrow 9/2^+$	1453
112.0	c		−0.20(3)	−0.07(5)	$3/2^+ \rightarrow 1/2^+$	112
118.6	123(20) [d]	1.08(17) ΣD	−0.33(4)	+0.08(5)	$27/2^- \rightarrow 25/2^-$	3443
132.4	153(37)	0.97(15) D	−0.34(6)	−0.09(8)	$9/2^- \rightarrow 11/2^-$	589
155.6	c	0.94(15) D	−0.18(3)	−0.03(4)	$5/2^+ \rightarrow 3/2^+$	267
189.9	198(31)	0.53(10) Q	f		$7/2^+ \rightarrow 5/2^+$	721
190.2	c		f		$11/2^- \rightarrow 5/2^+$	457
209.9	296(35)	0.79(10) Q	−0.19(1)	−0.08(2)	$23/2^+ \rightarrow 21/2^+$	2866
214.8	491(55)	0.52(5) Q	−0.20(1)	−0.06(1)	$27/2 \rightarrow 25/2^+$	3312
222.8	17(6)	1.98(80) D			$29/2 \rightarrow 25/2$	3552
223.9	c				$3/2^+ \rightarrow 1/2^+$	224
227.2	17(5)	1.02(20) ΣD			$25/2^- \rightarrow 25/2^+$	3325
232.3	201(25)	0.94(10) D	−0.22(2)	−0.02(3)	$25/2^+ \rightarrow 23/2^+$	3098
243.8	42(9)	1.21(25) D			$35/2 \rightarrow 33/2$	5406
251.1	9(3)				$35/2 \rightarrow 35/2$	4692
260.1	90(11)	1.13(20) [g]			$19/2^+ \rightarrow 17/2^+$	2548
263.9	40(11)				$5/2^+ \rightarrow 5/2^+$	531
265.0	245(27)	1.03(9) D			$29/2^- \rightarrow 27/2^-$	3708
267.6	c	1.09(10) Q			$5/2^+ \rightarrow 1/2^+$	267
270.0	87(15)	2.01(25) D			$29/2 \rightarrow 25/2$	3552
271.8	87(10)	0.81(20) Q			$9/2^+ \rightarrow 9/2^+$	1346
302.0	8(3)	0.85(25) Q			$43/2 \rightarrow 39/2$	5708
319.0	64(13)	1.10(15) D			$37/2 \rightarrow 35/2$	5725
337.3	202(23)	0.97(7) D			$31/2^- \rightarrow 29/2^-$	4045
342.3	17(4)				$21/2^+ \rightarrow 19/2^+$	2907
344.5	17(5)	0.80(27) ΣD			$27/2^- \rightarrow 25/2^+$	3443
368.0	449(46)	0.96(10) Q	+0.13(1)	−0.01(2)	$21/2^+ \rightarrow 17/2^+$	2656
379.7	205(23)	1.01(7) Q	+0.15(5)	−0.21(7)	$13/2^+ \rightarrow 9/2^+$	1453
383.5	11(4)				$29/2^- \rightarrow 25/2^-$	3708
384.2	348(36)	2.05(18) D	+0.46(2)	−0.12(3)	$23/2^+ \rightarrow 19/2^+$	2581
392.4	25(6)	0.79(35) Q			$39/2 \rightarrow 35/2$	5083
395.1	29(6)	0.82(25) D			$39/2 \rightarrow 37/2$	6120
399.3	49(11)	1.02(15) D			$39/2 \rightarrow 37/2$	6124
409.4	111(15)	0.95(10) D			$33/2^- \rightarrow 31/2^-$	4454
410.4	129(14)	0.93(10) Q			$17/2^+ \rightarrow 13/2^+$	2289
410.4	129(14)	0.93(10) Q			$17/2^+ \rightarrow 13/2^+$	2289
416.5	431(43)	1.86(20) D	+0.26(2)	+0.07(2)	$11/2^+ \rightarrow 7/2^+$	1137
419.5	420(42)	0.52(5) Q			$19/2^+ \rightarrow 17/2^-$	2197
420.3	181(31)	1.19(25) D			$5/2^+ \rightarrow 3/2^+$	531
421.0	452(50)	1.02(7) Q			$31/2 \rightarrow 27/2$	3732
434.1	110(13)	0.89(15) Q			$23/2^- \rightarrow 23/2^-$	3253
441.9	487(54)	1.08(10) Q	+0.12(2) [h]	−0.05(3) [h]	$25/2^+ \rightarrow 21/2^+$	3098
453.8	205(32)	0.57(10) Q	−0.72(3)	+0.51(4)	$7/2^+ \rightarrow 5/2^+$	721
460.1	63(18)	0.87(30) Q			$(33/2) \rightarrow 29/2$	4012
470.9	20(7)				$19/2^- \rightarrow 17/2^-$	2248
472.6	65(12)	0.96(9) ΣD			$35/2^- \rightarrow 33/2^-$	4927
477.5	15(5)				$\rightarrow 9/2^-$	1066
481.0	62(12)	1.87 [i]			$27/2^+ \rightarrow 23/2^+$	3346
490.7	38(8)	1.01(20) D			$41/2 \rightarrow 39/2$	6614
491.3	15(4)				$(39/2) \rightarrow 37/2^-$	5933
494.5	15(5)	0.90(25) ΣD			$41/2 \rightarrow 39/2$	6614
506.4	67(13)	1.09(13) ΣD			$25/2^- \rightarrow 23/2^-$	3325

TABLE I. (*Continued*).

E_γ (keV)	I_γ [a]	DCO [b]	A_2	A_4	$J_i^\pi \rightarrow J_f^\pi$	E_x (keV)
509.3	535(54)	0.72(10) Q			$17/2^+ \rightarrow 15/2^+$	2289
513.5	34(7)	1.05(11) ΣD			$37/2^- \rightarrow 35/2^-$	5440
514.0	279(29)	0.98(7) Q	+0.14(2)	−0.02(3)	$17/2^+ \rightarrow 13/2^+$	1967
515.8	56(6)	0.52(8) Q			$15/2^- \rightarrow 13/2^-$	1580
519.5	55(15)	0.65(18) ΣQ			$33/2 \rightarrow 31/2$	4879
526.0	20(6)	0.90(20) ΣD			$35/2 \rightarrow 33/2$	5406
531.5	45(10)	1.89(15) D			$5/2^+ \rightarrow 1/2^+$	531
534	8(4)				$15/2^- \rightarrow 15/2^-$	1580
542.5	53(15)	0.53(15) ΣQ			$33/2 \rightarrow 31/2^+$	4879
547.4	322(32)	0.94(10) D	−0.15(1)	+0.05(2)	$11/2^+ \rightarrow 9/2^-$	1137
550.7	23(5)	0.43(11) Q			$41/2 \rightarrow 39/2$	5957
560.0	12(4)				$(41/2) \rightarrow (39/2)$	6501
560.5	12(4)	1.17(25) ΣD			$43/2 \rightarrow 41/2$	7174
577.2	27(9)	0.89(25) ΣD			$43/2 \rightarrow 41/2$	7191
583.5	69(13)	0.48(7) Q			$23/2^- \rightarrow 21/2^-$	3253
590.0	1000	1.01(5) Q	+0.31(1)	−0.08(2)	$15/2^- \rightarrow 11/2^-$	1047
601.9	59(9)				$31/2^- \rightarrow 27/2^-$	4045
608.2	270(32)	0.37(8) Q	−1.19(12)	+0.27(17)	$13/2^- \rightarrow 11/2^-$	1065
609.5	112(14)	0.94(10) Q			$25/2^+ \rightarrow 21/2^+$	3516
618.5	116(15)	1.03(10) Q			$21/2^+ \rightarrow 17/2^+$	2907
625.3	128(15)	0.96(8) Q			$43/2 \rightarrow 39/2$	5708
625.4	18(5)	1.70(40) ΣD			$27/2^- \rightarrow 23/2^-$	3443
643.7	660(71)	1.10(19) Q	j		$15/2^+ \rightarrow 11/2^+$	1780
644.1	253(28)	0.94(9) Q	j		$39/2 \rightarrow 35/2$	5083
646.2	99(14)	1.02(10) Q			$29/2^+ \rightarrow 25/2^+$	4162
656	7(4)				$25/2^- \rightarrow 21/2^-$	3325
662.0	15(5)				$\rightarrow 51/2$	8062
668.5	42(6)	2.04(25) D			$19/2^- \rightarrow 15/2^-$	2248
669.1	20(6)				$25/2^- \rightarrow 21/2^+$	3325
680.0	74(10)	1.04(9) Q			$33/2^+ \rightarrow 29/2^+$	4841
682.5	43(10)	1.03(12) Q			$41/2 \rightarrow 37/2$	5957
689.5	275(29)	1.02(10) Q			$21/2^+ \rightarrow 17/2^+$	2656
701.3	15(5)				$\rightarrow 51/2$	8062
701.6	136(16)	0.46(6) Q			$25/2 \rightarrow 23/2^+$	3282
708.1	341(39)	0.99(7) Q			$35/2 \rightarrow 31/2$	4440
708.4	10(3)				$17/2^+ \rightarrow 15/2^-$	2289
713.5	15(5)				$15/2^+ \rightarrow$	1780
713.7	166(17)	1.82(25) D			$17/2^- \rightarrow 13/2^-$	1778
722.0	15(4)	1.50(75) D			$37/2^+ \rightarrow 33/2^+$	5576
731.6	440(31)	0.27(3) Q	−0.83(2)	+0.06(3)	$17/2^- \rightarrow 15/2^-$	1778
734.6	70(10)	0.97(10) Q			$37/2^+ \rightarrow 33/2^+$	5576
740	10(3)	1.06(20) D			$35/2 \rightarrow 33/2$	5319
742.1	137(15)	0.61(11) Q			$13/2^+ \rightarrow 11/2^+$	1879
746.6	40(8)				$33/2^- \rightarrow 29/2^-$	4454
748.6	50(10)	0.41(19) Q			$25/2 \rightarrow 23/2^+$	3329
775.6	46(12)	1.14(15) Q			$31/2^+ \rightarrow 27/2^+$	4121
775.8	88(13)	1.04(9) Q			$47/2 \rightarrow 43/2$	6484
784.3	28(5)				$31/2^+ \rightarrow 29/2$	4336
786.2	57(6)	1.08(25) Q			$19/2^+ \rightarrow 15/2^+$	2565
787.5	30(9)				$21/2^+ \rightarrow 19/2^-$	2656
800.5	98(13)	0.54(9) Q			$21/2^- \rightarrow 19/2^-$	2670
807.5	349(36)	0.98(7) Q			$9/2^+ \rightarrow 5/2^+$	1074
807.9	77(8)	1.02(11) Q			$41/2^+ \rightarrow 37/2^+$	6384
808.3	31(7)	1.22(40) ΣD			$31/2^+ \rightarrow 29/2$	4359
822.9	481(34)	0.98(6) Q	+0.26(2)	−0.17(3)	$19/2^- \rightarrow 15/2^-$	1869
827.7	137(16)	1.01(11) Q			$27/2^+ \rightarrow 23/2^+$	3408

TABLE I. (*Continued*).

E_γ (keV)	I_γ [a]	DCO [b]	A_2	A_4	$J_i^\pi \rightarrow J_f^\pi$	E_x (keV)
835.2	31(8)	1.67(50) D			29/2 →25/2	4118
835.4	46(6)	0.61(15) Q			37/2 →35/2	5275
846.3	39(6)	0.55(10) Q			33/2 →31/2	4578
877.8	32(6)	0.84(20) ΣQ			51/2 →47/2	7361
880.1	8(3)				(55/2) →51/2	8281
882.3	46(9)				$35/2^-$ →$31/2^-$	4927
885.7	31(6)	0.91(15) ΣQ			$45/2^+$ →$41/2^+$	7270
891.9	69(10)	2.09(35) D			$21/2^-$ →$17/2^-$	2670
902.6	23(5)	1.04(18) ΣQ			$49/2^+$ →$45/2^+$	8173
908.0	19(5)	0.95(18) ΣQ			$53/2^+$ →$49/2^+$	9081
917.0	43(8)	0.96(10) Q			51/2 →47/2	7401
928.1	70(12)	0.98(9) Q			$31/2^+$ →$27/2^+$	4336
937.6	34(7)	1.05(15) Q			45/2 →41/2	6894
950.1	237(24)	0.97(7) Q			$23/2^-$ →$19/2^-$	2819
952.1	60(13)	1.35(40) Q			$31/2^+$ →$27/2^+$	4359
960.0	25(6)	0.85(40) Q			35/2 →31/2	4692
967.4	67(11)	0.98(12) Q			39/2 →35/2	5406
969.9	16(5)	1.08(22) ΣQ			$57/2^+$ →$53/2^+$	10051
986.2	23(6)				$37/2^-$ →$33/2^-$	5440
987	8(3)					7229
1005.0	34(10)				(39/2) →$35/2^-$	5933
1005.2	76(13)	2.15(25) ΣD			$23/2^-$ →$19/2^-$	3253
1014.8	10(3)				→39/2	6097
1021.2	13(4)	1.07(30) Q			$35/2^+$ →$31/2^+$	5142
1039.4	12(4)	1.05(77) Q			(39/2) →35/2	5480
1044	9(3)				33/2 →29/2	5162
1051.4	15(5)				(41/2) →$37/2^-$	6501
1061.0	15(4)	0.90(26) ΣQ			$61/2^+$ →$57/2^+$	11113
1066	10(3)				→39/2	6149
1079.0	53(6)	0.96(15) Q			$9/2^+$ →$5/2^+$	1346
1108.0	15(4)	0.51(15) Q			$33/2^+$→31/2	4841
1108.5	8(4) [d]				(59/2) →(55/2)	9390
1118	9(3)				→51/2	8519
1120.7	20(5)	0.55(18) Q			$33/2^+$ →31/2	4853
1131	11(3)				(49/2) →45/2	8025
1159	14(4)				→39/2	6242
1189.9	11(3)				→39/2	6595
1201.7	19(7)				$19/2^-$→ $15/2^-$	2248
1242.9	18(4)	0.48(15) Q			$17/2^+$→ $15/2^-$	2289
1384.2	94(11)	0.96(10) Q	+0.30(5)	−0.15(7)	$23/2^-$→ $19/2^-$	3253

[a]The relative intensities were determined from the thick-target experiment (the exceptions are noted) and were normalized to the 590.0 keV $15/2^- \rightarrow 11/2^-$ transition.

[b]The meaning of the capital letters is D, gate set on a stretched dipole transition; Q, gate set on a stretched quadrupole transition; ΣD, gates set on a sum of consecutive stretched dipole transitions; ΣQ, gates set on a sum of consecutive stretched quadrupole transitions.

[c]The intensity of the transitions below the isomer state is not determined from the present measurement. The arrow thickness of these transitions in Fig. 2 is obtained assuming zero sidefeeding for the corresponding levels.

[d]Intensity obtained from the thin-target experiment.

[e]$A_2 = +0.10(9)$, $A_4 = 0$ for the 108.2+108.3 keV γ rays.

[f]$A_2 = -0.05(3)$, $A_4 = -0.09(4)$ for the 189.9+190.2 keV γ rays.

[g]Extracted by gating on the 509.3 keV *dipole*-quadrupole mixed transition.

[h]Corrected for 50% contribution from an analogous 441.9 keV $E2$ transition in ^{140}Sm.

[i]Extracted by gating on the 209.9 keV *dipole*-quadrupole mixed transition.

[j]$A_2 = +0.11(2)$, $A_4 = +0.06(2)$ for the 643.7+644.1 keV γ rays.

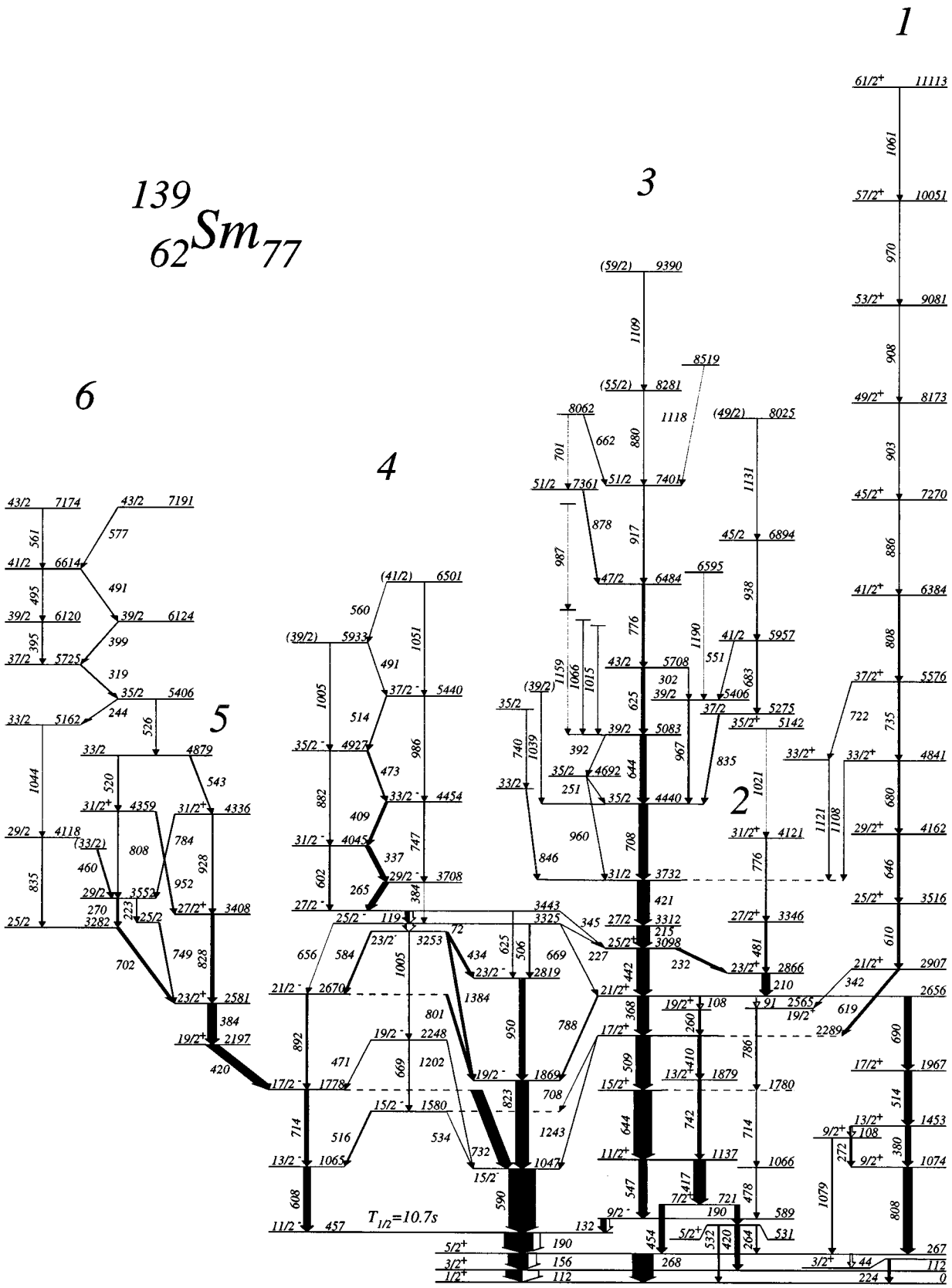

FIG. 2. Level scheme of ^{139}Sm obtained from the present experiments. The width of the arrows is proportional to the transition intensity.

^{137}Nd. In ^{139}Sm the corresponding state (with $T_{1/2} < 1$ ns) decays through a 419.5 keV transition which has a DCO ratio of 0.5, typical of a pure $\Delta I = 1$ transition with $E1$ character. For comparison, the DCO ratios of the 608.2 and 731.6 keV transitions, of mixed $M1+E2$ character, are 0.37 and 0.27, respectively (see Table I). Built on the state at 2197 keV a sequence of three transitions of stretched quadrupole character is observed, which defines spin $31/2^+$ for the state at 4336 keV belonging to the structure labeled 5.

Above the $23/2^-$ level at 3253 keV the regularity of the structure built on the $11/2^-$ isomer is broken and we may also face a change of parity. In this particular case, we could establish the parity of the band built above from intensity balance considerations. We could in fact extract the conversion coefficients for the 72.2 and 118.6 keV transitions depopulating the states at 3325 and 3443 keV, respectively. The values $\alpha(72.2)_{\text{expt}} = 3.8(11)$ and $\alpha(118.6)_{\text{expt}} = 1.02(8)$ have been obtained from the analysis of a clean double-gated spectrum with gates set on the transitions belonging to the upper part of the band. The experimental values are in good agreement with the theoretical ones only in the case of $M1$ transitions, for which one obtains $\alpha(72.2)_{\text{th}} = 4.37$ and $\alpha(118.6)_{\text{th}} = 1.05$, respectively.

A change of parity is possible also above the level with spin $25/2^+$ at 3098 keV in the structure labeled 3 in Fig. 1. A strong transition of 214.8 keV with angular distribution coefficients and DCO ratio typical of a pure $\Delta I = 1$ transition is populating that level. The experimental information is not sufficient anyway to establish the parity of the states above $E_x = 3098$ keV.

IV. DOPPLER SHIFT ATTENUATION METHOD ANALYSIS

The data of the thick-target experiment have also been analyzed in order to obtain lifetime information by applying the Doppler shift attenuation method (DSAM). For this purpose five γ-γ matrices were created, having on one axis the detectors lying at one specific angle (34°, 60°, 90°, 120°, and 146°) with respect to the beam direction and on the other axis the remaining detectors. The spectra of interest for the DSAM analysis were obtained by gating on appropriate transitions in the lower part of the various structures of ^{139}Sm.

Only transitions belonging to the HD band showed Doppler broadening. The line-shape analysis has been performed for the 807.9, 885.7, 902.6, 908.0, 969.9, and 1061.0 keV transitions of that band. Spectra corresponding to the above-mentioned angles were produced by gating on the lowest in band transitions (609.5, 646.2, 680.0, and 734.6 keV) which did not show any Doppler broadening. The best spectrum for every analyzed transition was obtained by summing only those gates which do not bring too many contaminant lines in the energy region of interest. For the lifetime analysis the code DSAMFT [22] has been used, which allows simultaneous line-shape fits of the data at all angles. The Monte Carlo simulation of the velocity distributions has been performed by using the stopping powers of Ziegler [23]. The sidefeeding into each state was approximated by a rotational band of five transitions, assumed to have the same moment of inertia and quadrupole moment as the main band. Unfortunately, many of the transitions which show Doppler broadening are contaminated and lie on a rather high background. Moreover, due to the small energy difference between the 902.6 and 908.0 keV transitions the corresponding peaks overlap. Figure 3 illustrates the cleanest experimental line shapes at forward and backward angles for the 807.9 and 969.9 keV transitions, together with the corresponding least-squares fits. This analysis allowed to determine for the quadrupole moment of the intruder band a value of $Q_0 = 3.9(7)$ e b.

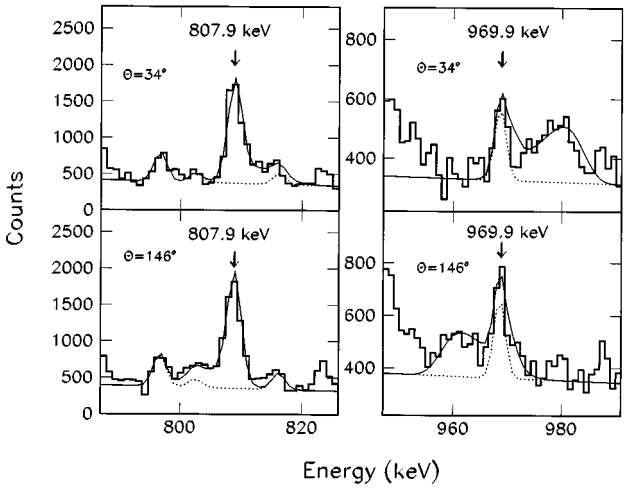

FIG. 3. Examples of line-shape analysis for the transitions of 807.9 and 969.9 keV of the $i_{13/2}$ intruder band. Dotted line: fit of the background and of contaminant lines. Solid line: global fit.

V. DISCUSSION

The level scheme of ^{139}Sm, as deduced from the present work, displays a very complicated structure up to an excitation energy of about 2.5 MeV, whereas above that energy regular structures develop (labeled from 1 to 6). In the following we describe in detail the low-spin part of the level scheme in the framework of the interacting boson-fermion model. The extension of the model to include broken pairs allows also a description of high-spin states, and in particular calculations are performed for the band labeled 4. Of the other high-spin structures, the one built on the $19/2^+$ state can also be understood using the same formalism, even if a quantitative comparison between experiment and theory could not be done. The intruder band based in the $\nu i_{13/2}$ orbital is outside the theoretical framework used and will be discussed in terms of the cranked shell model. For the other high-spin states it is difficult to give an interpretation, since the parity is not known (see, e.g., the case of the structures labeled 3 and 6 in Fig. 2).

A. Interacting boson-fermion model plus broken pairs interpretation

Models of nuclear structure that are based on the interacting boson approximation (IBA) [24] provide a unified framework for the description of medium heavy and heavy nuclei. Among the many extensions [24,25] of the original interacting boson model (IBM-1) [26], there are also those which include the physics of high-spin states. In order to describe

high-spin states in nuclei ($10\hbar \leqslant J \leqslant 30\hbar$), one has to go beyond the interacting boson approximation and to extend the model space by including, in addition to bosons, part of the original shell model space for valence nucleons. This is done by breaking the correlated S and D pairs (s and d bosons) to form selective noncollective fermion pairs. In this way, high angular momentum states can be generated and their structure described by the coupling between fermions in broken pairs and the bosonic core.

In Refs. [7,8,27–33] an extension of the IBM has been investigated that includes two- and four-fermion noncollective states (one and two broken pairs). The model has been applied to the description of high-spin states in the Hg [7,8,30], Sr-Zr [29,31,32], and Nd-Sm [33] regions. In Ref. [8] the interacting boson-fermion model for odd nuclei has been extended to include one broken pair. The model is completely equivalent to the one used for even nuclei, and is based on the simplest version of the interacting boson-fermion model: the IBFM-1 [6]. The model space for an odd-even nucleus with $2N+1$ valence nucleons reads

$$|(N)\text{bosons}\otimes 1\text{fermion}\rangle \oplus |(N-1)\text{bosons}\otimes 1\text{broken pair}\otimes 1\text{fermion}\rangle.$$

In the IBFM-1 one does not distinguish between proton and neutron bosons. Here, however, there are two possibilities for the fermion subspace: (i) the two fermions in the broken pair can be of the same type as the unpaired fermion, resulting in a space with three identical fermions; (ii) if the fermions in the broken pair are different from the unpaired fermion, the fermion basis contains two protons and one neutron or vice versa. Although generally the fermions in broken pairs occupy all the valence single-particle orbitals from which the bosons have been mapped, for the description of high-spin states close to the yrast line the most important are the unique parity orbitals. For the case where the three-fermion basis consists of identical nucleons, the model Hamiltonian is identical to that of the corresponding even-even nucleus

$$H = H_B + H_F + V_{BF} + V_{\text{mix}}. \tag{5.1}$$

H_B is the boson Hamiltonian of IBM-1 [24]:

$$\begin{aligned} H_B = {} & \epsilon \hat{n}_d + \sum_{L=0,2,4} \frac{1}{2}\sqrt{2L+1}\, c_L [(d^\dagger \times d^\dagger)^{(L)} \times (\tilde{d}\times\tilde{d})^{(L)}]^{(0)} \\ & + \frac{1}{\sqrt{2}} v_2 \{[(d^\dagger \times d^\dagger)^{(2)} \times (\tilde{d}\times s)^{(2)}]^{(0)} + \text{H.c.}\} \\ & + \frac{1}{2} v_0 \{[(d^\dagger \times d^\dagger)^{(0)} \times (s\times s)^{(0)}]^{(0)} + \text{H.c.}\}. \end{aligned} \tag{5.2}$$

The fermion Hamiltonian H_F contains the single-fermion energies and fermion-fermion interactions

$$H_F = \sum_\alpha E_\alpha a^\dagger_\alpha a_\alpha + \frac{1}{4}\sum_{abcd}\sum_{JM} V^J_{abcd} A^\dagger_{JM}(ab) A_{JM}(cd), \tag{5.3}$$

where the fermion pair operator is defined as

$$A^\dagger_{JM}(ab) = \frac{1}{\sqrt{1+\delta_{ab}}} [a^\dagger_a \times a^\dagger_b]^{(J)}_M. \tag{5.4}$$

The first part of the interaction between the unpaired fermions and the boson core is the IBFM-1 boson-fermion interaction [25,6]

$$V_{BF} = V_{\text{dyn}} + V_{\text{exc}} + V_{\text{mon}}. \tag{5.5}$$

The quadrupole-quadrupole dynamical interaction is

$$\begin{aligned} V_{\text{dyn}} = {} & \Gamma_0 \sum_{j_1 j_2} (u_{j_1} u_{j_2} - v_{j_1} v_{j_2}) \langle j_1 \| Y_2 \| j_2 \rangle \\ & \times ([a^\dagger_{j_1} \times \tilde{a}_{j_2}]^{(2)} \cdot Q^B), \end{aligned} \tag{5.6}$$

where the boson quadrupole operator is defined by

$$Q^B = [s^\dagger \times \tilde{d} + d^\dagger \times \tilde{s}]^{(2)} + \chi [d^\dagger \times \tilde{d}]^{(2)}. \tag{5.7}$$

The exchange and monopole terms of the boson-fermion interaction are, respectively,

$$\begin{aligned} V_{\text{exc}} = {} & -\Lambda_0 2\sqrt{5} \sum_{j_1 j_2 j_3} (2j_3+1)^{-1/2} (u_{j_1} v_{j_3} + v_{j_1} u_{j_3}) \\ & \times (u_{j_2} v_{j_3} + v_{j_2} u_{j_3}) \langle j_3 \| Y_2 \| j_1 \rangle \langle j_3 \| Y_2 \| j_2 \rangle \\ & \times :[(a^\dagger_{j_1} \times \tilde{d})^{(j_3)} \times (\tilde{a}_{j_2} \times d^\dagger)^{(j_3)}]^{(0)}: \end{aligned} \tag{5.8}$$

and

$$V_{\text{mon}} = A_0 \sqrt{5} \sum_j (2j+1) ([a^\dagger_j \times \tilde{a}_j]^{(0)} \cdot [d^\dagger \times \tilde{d}]^{(0)}). \tag{5.9}$$

The terms H_B, H_F, and V_{BF} of the Hamiltonian (1) conserve the number of bosons and the number of fermions separately. In our model only the total number of nucleons is conserved, bosons can be destroyed, and fermion pairs created, and vice versa. In the same order of approximation as for V_{BF}, the pair breaking interaction V_{mix} which mixes states with different number of fermions, conserving the total nucleon number only, reads

$$\begin{aligned} V_{\text{mix}} = {} & -U_0 \Bigg\{ \sum_{j_1 j_2} u_{j_1} u_{j_2} (u_{j_1} v_{j_2} + u_{j_2} v_{j_1}) \\ & \times \langle j_1 \| Y_2 \| j_2 \rangle^2 \frac{1}{\sqrt{2j_2+1}} ([a^\dagger_{j_2} \times a^\dagger_{j_2}]^{(0)} \cdot s) + \text{H.c.} \Bigg\} \\ & - U_2 \Bigg\{ \sum_{j_1 j_2} (u_{j_1} v_{j_2} + u_{j_2} v_{j_1}) \langle j_1 \| Y_2 \| j_2 \rangle \\ & \times ([a^\dagger_{j_1} \times a^\dagger_{j_2}]^{(2)} \cdot \tilde{d}) + \text{H.c.} \Bigg\}. \end{aligned} \tag{5.10}$$

If the three-fermion basis consists of proton and neutron states (the broken-pair nucleons and the odd nucleon are of

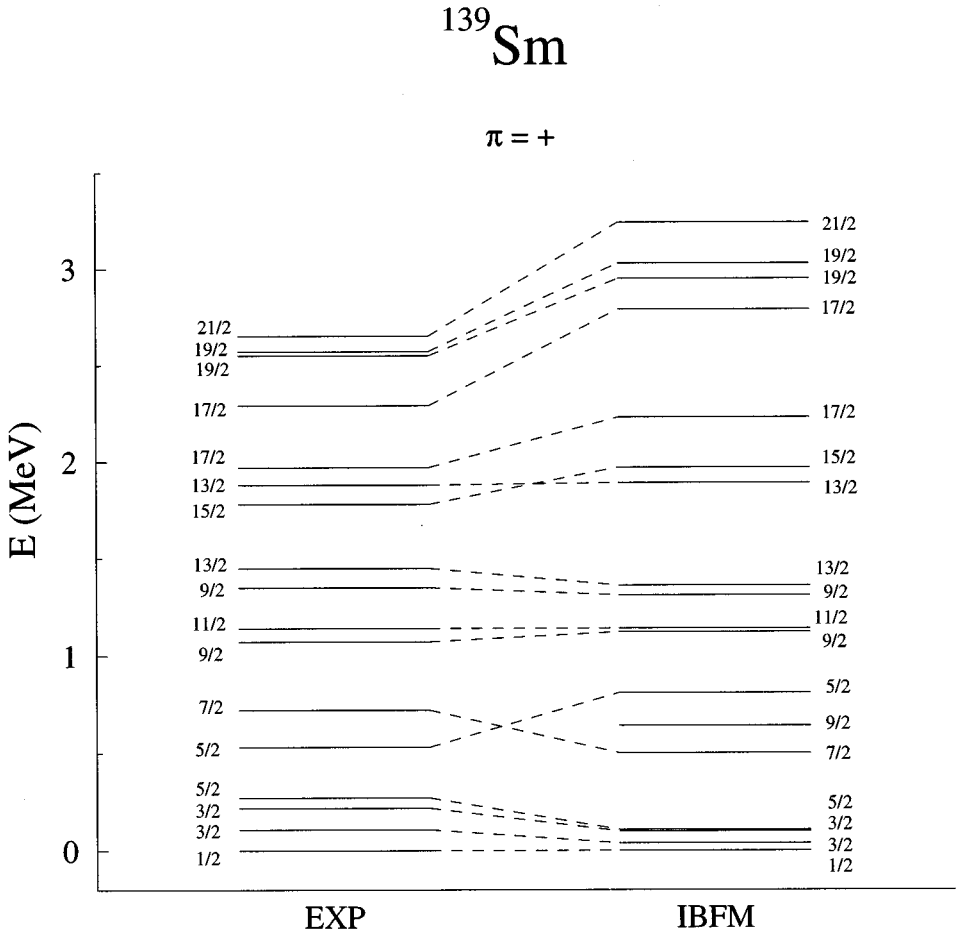

FIG. 4. Comparison between the experimental excitation energies of low-lying positive-parity states in ^{139}Sm and the levels calculated in the interacting boson-fermion model.

opposite type), there will be two H_F and two V_{BF} terms in the Hamiltonian (5.1). In this case calculations are more complicated. There are, for instance, more parameters that have to be adjusted in order to reproduce the experimental spectrum. In general, most of the parameters of the Hamiltonian are taken from analyses of the low- and high-spin states in the neighboring even and odd nuclei.

For ^{139}Sm the core nucleus is ^{140}Sm. The structure of two- and four-quasiparticle high-spin bands in ^{140}Sm has been recently described in the framework of the interacting boson model plus one- and two-broken pairs [34]. The set of parameters of the boson Hamiltonian is $\epsilon=0.38$, $C_0=0.2$, $C_2=-0.036$, $C_4=0.16$, $V_2=0$, and $V_0=-0.2$ (all values in MeV). The number of bosons is $N=8$. The boson parameters have values similar to those used in the calculation of ^{138}Nd [33]. The resulting spectrum is close to the O(6) dynamical symmetry limit.

The structure of high-spin states in $A\approx140$ nuclei close to the yrast line is characterized by the alignment of both proton and neutron pairs in the $h_{11/2}$ orbital. Two $\Delta I=2$ bands based on the first and second 10^+ states are seen in ^{140}Sm. The measured g factors of these 10^+ states [35] indicate a two-neutron $(\nu h_{11/2})^2$ configuration for the band built on the yrast 10^+ state and a two-proton configuration $(\pi h_{11/2})^2$ for the band based on the second 10^+ state at 3210 keV. As compared to ^{138}Nd, the ^{140}Sm nucleus has two more protons; the proton Fermi level is accordingly higher and less energy is needed to promote protons in the $h_{11/2}$ orbit. Consequently, the $(\pi h_{11/2})^2$ band is $\approx$ 500 keV lower in ^{140}Sm while the $(\nu h_{11/2})^2$ band does not change its position.

For the positive-parity states in ^{139}Sm we have performed an interacting boson-fermion calculation. For the description of the negative-parity states and, in particular, of the structure labeled 4 in Fig. 2 the extended version of the model, with one broken pair, has been used. As a result, this high-spin structure is described as a three-neutron $(\nu h_{11/2})^3$ band. The alternative configuration $\nu h_{11/2}\otimes(\pi h_{11/2})^2$ has been also investigated but, in this case, no correspondence is found between calculated and experimental levels. The neutron orbitals included in the calculation are $d_{3/2}$, $s_{1/2}$, $g_{7/2}$ for positive-parity states, and $h_{11/2}$ for negative-parity states. In the $N=79$, 81 nuclei, the $1/2^+_1$ state (predominantly $s_{1/2}$ quasiparticle state) is very low in energy. For these nuclei the reported IBFM calculations [36–39] employed quasiparticle energies and occupation probabilities obtained from a simple BCS calculation using the Kisslinger-Sorensen parametrization [40]. An additional shift of the $s_{1/2}$ single-particle energy was found necessary in order to obtain a low-lying $1/2^+$ state. On the other hand, in the $N=73$ nuclei ^{131}Ce and ^{132}Pr [41,42], a Reehal-Sorensen parametrization [43] was used. This parametrization produces low-lying $s_{1/2}$ and $g_{7/2}$ quasiparticle states, in agreement with the experimental data. For $N=77$ nuclei like ^{139}Sm, a reasonable choice of single-particle energies would be somewhere between those used

for $N=73$ and $N=79$, 81. We have used a Kisslinger-Sorensen parametrization with additional single-particle energy shifts: +1.0 MeV for $s_{1/2}$, −0.7 MeV for $h_{11/2}$, and +0.2 MeV for $d_{3/2}$. Using a pairing strength of $G=(23/A)$ MeV, the resulting quasiparticle energies and occupation probabilities are $E(\nu d_{3/2})=0.78$ MeV, $E(\nu s_{1/2})=0.84$ MeV, $E(\nu h_{11/2})=1.14$ MeV, $E(\nu g_{7/2})=2.05$ MeV, $v^2(\nu d_{3/2})=0.38$, $v^2(\nu s_{1/2})=0.71$, $v^2(\nu h_{11/2})=0.87$, $v^2(\nu g_{7/2})=0.96$. In Fig. 4 we display the results of model calculations for positive-parity states and compare them with the experimental levels of the same parity. The few lowest calculated levels of each spin that have a possible experimental counterpart are shown. Above 1 MeV the density of calculated levels is relatively high and therefore they could not be all included in the figure. The parameters of the boson-fermion interactions are $\Gamma_0=0.03$ MeV and $\chi=-1$ for the dynamical interaction, $A_0=0.08$ MeV for the monopole interaction, and $\Lambda_0=1.4$ MeV for the exchange interaction. Table II gives the wave functions of the states up to $15/2_1^+$ which are believed to contain negligible three-fermion amplitudes. We notice that the calculated positive-parity states reproduce the experimental level structure up to approximately 2 MeV excitation energy (spin $17/2^+$). Above 2 MeV the experimental level scheme is very complicated and one expects larger contributions from three-quasiparticle states. However, the three-fermion positive-parity bases which include the $h_{11/2}$ orbital are prohibitively large. We present therefore only results with one unpaired fermion.

For the negative-parity states close to the yrast line, the systematics of this nuclear region indicates that the most important contribution comes from the $h_{11/2}$ neutron orbital. For the description of the structure labeled 4 in Fig. 2, we performed an IBFM plus broken pairs calculation including only the $h_{11/2}$ orbital in the one- plus three-fermion basis. As for ^{138}Nd [33] and for ^{140}Sm [34], the single-quasiparticle energy $E_{\nu h11/2}\approx$ 1.1 MeV is too low. In order to reproduce the excitation energies of the 10_1^+ states in the two even-even nuclei, we had to renormalize the value of $E_{\nu h11/2}$ to 1.6 MeV. For ^{139}Sm we take $E_{\nu h11/2}=1.65$ MeV. Since the fermion space for negative-parity states (the $h_{11/2}$ orbital) is different from that taken for the positive-parity states ($d_{3/2}$, $s_{1/2}$, $g_{7/2}$) the adopted boson-fermion interaction parameters are also different being now $\Gamma_0=0.3$ MeV, $\chi=-1$, $A_0=0.02$ MeV. The strength parameter of the pair breaking interaction is $U_2=0.2$ MeV. The residual interaction between unpaired neutrons is a surface δ interaction with a strength parameter $v_0=-0.1$ MeV. This choice of parameters is very close to the values that we have used in the neighboring even- and odd-A nuclei to describe the states involving the $h_{11/2}$ neutron orbital [33,34]. The only difference in the present calculations is that the exchange term of the boson-fermion interaction is not included. This is done in order to obtain a better description of the three-neutron band based on the state $27/2_1^-$. With the exchange term one obtains a better agreement between calculated and experimental low-spin one-neutron states, but the three-neutron band consists of almost degenerate doublets. This anomaly was also observed in the calculation of four-quasiparticle bands in ^{86}Zr [29] and ^{140}Sm [34], and has been discussed in Refs. [31,32].

TABLE II. IBFM wave functions of positive-parity states in ^{139}Sm. The basis states are $|lj,n_sn_dI;J\rangle$ and the corresponding amplitudes are given in the last column. Only components with amplitudes $\geqslant 4\%$ are included in the table.

J_k^π	lj	n_d	I	ξ
$1/2_1^+$	$s1/2$	0	0	−0.65
	$s1/2$	2	0	−0.62
	$g7/2$	2	4	0.21
	$s1/2$	4	0	−0.31
$3/2_1^+$	$d3/2$	0	0	0.63
	$d3/2$	2	0	0.55
	$s1/2$	2	2	−0.24
	$d3/2$	2	2	−0.27
	$d3/2$	4	0	0.25
$3/2_2^+$	$s1/2$	1	2	0.69
	$g7/2$	1	2	0.28
	$s1/2$	3	2	0.54
	$g7/2$	3	2	0.25
	$s1/2$	5	2	0.21
$5/2_1^+$	$s1/2$	1	2	−0.40
	$d3/2$	1	2	−0.63
	$s1/2$	3	2	−0.31
	$d3/2$	3	2	−0.46
$5/2_2^+$	$s1/2$	2	2	0.59
	$g7/2$	2	4	−0.43
	$g7/2$	3	6	0.40
	$g7/2$	4	2	−0.31
$7/2_1^+$	$g7/2$	2	2	0.32
	$s1/2$	2	4	0.68
	$g7/2$	4	2	0.24
	$s1/2$	4	4	0.44
$9/2_1^+$	$g7/2$	2	2	0.24
	$s1/2$	2	4	−0.45
	$d3/2$	2	4	−0.66
	$s1/2$	4	4	−0.29
	$d3/2$	4	4	−0.40
$9/2_2^+$	$g7/2$	1	2	−0.66
	$g7/2$	3	2	−0.61
	$g7/2$	5	2	−0.27
$9/2_3^+$	$d3/2$	3	3	−0.32
	$g7/2$	3	3	0.25
	$s1/2$	3	4	−0.48
	$d3/2$	3	4	−0.45
	$g7/2$	3	4	0.32
	$s1/2$	5	4	−0.26
	$d3/2$	5	4	−0.22
$11/2_1^+$	$g7/2$	3	2	0.22
	$g7/2$	3	3	−0.28
	$g7/2$	3	4	0.22
	$s1/2$	3	6	0.72
	$s1/2$	5	6	0.38
$13/2_1^+$	$g7/2$	3	4	−0.27
	$s1/2$	3	6	0.47
	$d3/2$	3	6	0.68
	$s1/2$	5	6	0.25
	$d3/2$	5	6	0.35
$13/2_2^+$	$g7/2$	2	4	−0.70
	$g7/2$	4	4	−0.53
$15/2_1^+$	$g7/2$	4	4	−0.22
	$g7/2$	4	5	0.33
	$s1/2$	4	8	−0.76
	$s1/2$	6	8	−0.31

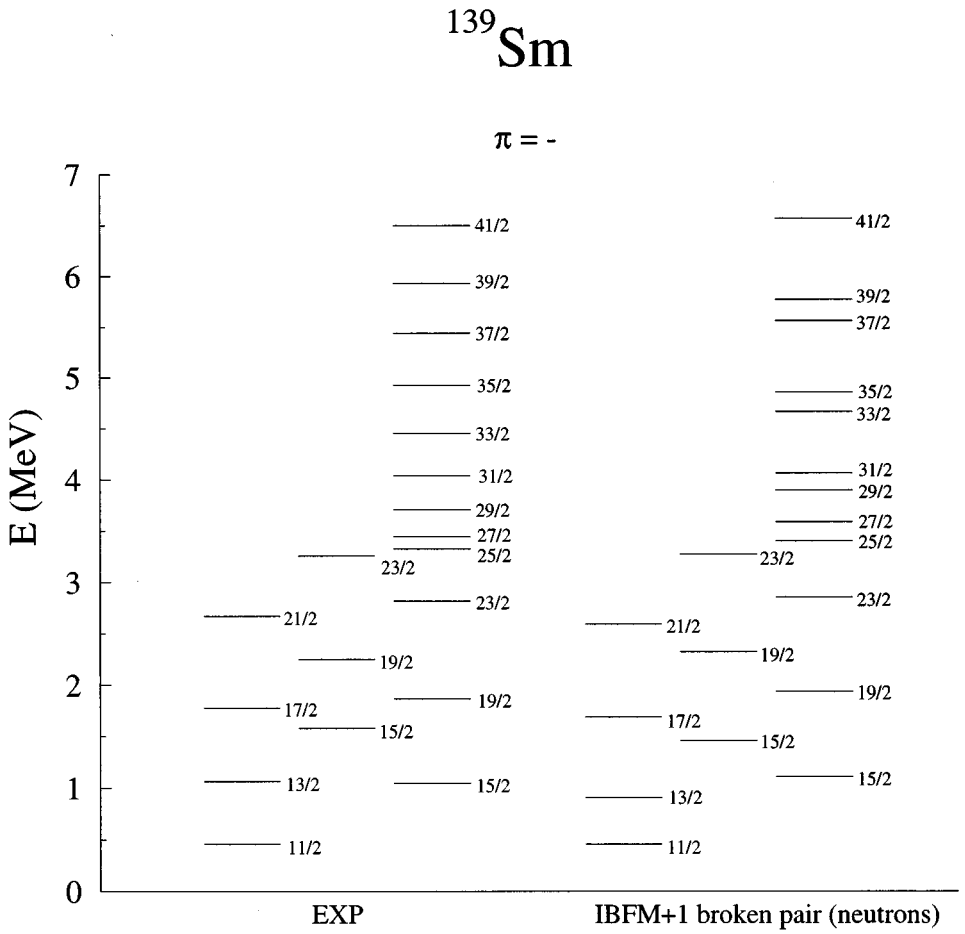

FIG. 5. Experimental and calculated negative-parity structure built on the $11/2^-$ isomer. For the description of the parameters used see text.

In Fig. 5 we compare the experimental and calculated negative-parity states which are based on the $h_{11/2}$ neutron orbital. In our calculation the states below $27/2_1^-$ represent one-neutron states and describe a decoupled structure typical for an O(6) core. The lowest structure is the decoupled band of favored states based on the $11/2_1^-$ state. The bandhead of the three-neutron structure is $27/2_1^-$. The excitation energy of this state relative to $11/2_1^-$ corresponds to the position of the isomer 10_1^+ in the core nucleus ^{140}Sm, on which the $(\nu h_{11/2})^2$ band is built. Compared with the positions of the experimental levels, we notice that the branch of favored states ($27/2_1^-$, $31/2_1^-$, $35/2_1^-$, $39/2_1^-$) is in excellent agreement with the experimental levels, while the branch ($29/2_1^-$, $33/2_1^-$, $37/2_1^-$, $41/2_1^-$) is somewhat higher. The structure of the wave functions corresponds to the lowest $(\nu h_{11/2})^2$ band in ^{140}Sm. The three $h_{11/2}$ neutrons are completely decoupled from the core and align their angular momenta along the axis of rotation. The maximum fermion angular momentum $j_F=27/2$ is a good quantum number for three-neutron states close to the yrast line. Close to the three-neutron yrast band we also expect to find the one-neutron–two-proton band $\nu h_{11/2}\otimes(\pi h_{11/2})^2$ with the bandhead having spin $31/2^-$. The structure of the band corresponds to the $(\pi h_{11/2})^2$ band in the core nucleus ^{140}Sm. However, we have not found any counterpart for such band in the level scheme.

In Table III we compare the calculated and experimental branching ratios for transitions between negative-parity states. The calculation reproduces the observed intensities for both the low-spin part of the spectrum (one-neutron states) and for transitions in the three-neutron structure based on the $27/2_1^-$ state. Disagreement between calculated and experimental intensities is found only in the band-crossing region, and in particular for the transitions deexciting the $23/2_2^-$, $25/2_1^-$, $27/2_1^-$ states. However, this is not unexpected since the density of states in this region is very high and the mixing in the wave functions of the calculated states so strong that it becomes very difficult to assign individual states. In the three-neutron band the $E2$ strengths start to dominate over the $M1$ ones above the $39/2_1^-$ state. In the calculations this effect occurs already for the $37/2_1^-$ state.

B. The positive-parity structure built on the $19/2^+$ level at 2197 keV

As already mentioned in Sec. III, isomeric $19/2^+$ states at $E_x\approx 2$ MeV are known in the $N=77$ isotones from ^{131}Xe up to ^{137}Nd. They have been interpreted as resulting from the coupling of a $h_{11/2}$ neutron to the 5^- states of $\nu s_{1/2}$ $(d_{3/2})$ $\otimes \nu h_{11/2}$ character, lying at comparable excitation energies in the neighboring even $N=78$ nuclei. In one case, ^{135}Ce, the g factor has been measured for the $19/2^+$ state [44], confirming its predominant $\nu s_{1/2}\otimes[\nu h_{11/2}]^2$ configuration. Sequences of stretched quadrupole transitions built on the $19/2^+$ and 5^- states have been identified in the odd-even

TABLE III. Calculated $B(E2)$ and $B(M1)$ strengths for transitions in ^{139}Sm. In the last two columns the experimental and theoretical branching ratios are given. The experimental values take into account the internal conversion.

E_x (keV)	$J_i^\pi \rightarrow J_f^\pi$	$B(E2)$ $(e^2\mathrm{b}^2)$	$B(M1)$ (μ_N^2)	I_{expt}	I_{IBFM}
1047	$15/2_1^- \rightarrow 11/2_1^-$	0.0659	–	100	100
1065	$13/2_1^- \rightarrow 15/2_1^-$	0.0551	0.2216	–	0.002
	$\rightarrow 11/2_1^-$	0.2244	0.2481	100	100
1580	$15/2_2^- \rightarrow 13/2_1^-$	0.2229	0.2387	100	100
	$\rightarrow 15/2_1^-$	0.0388	0.0120	14	8
	$\rightarrow 11/2_1^-$	0.0056	–	–	18
1778	$17/2_1^- \rightarrow 15/2_2^-$	0.0285	0.1839	–	1
	$\rightarrow 13/2_1^-$	0.0982	–	38	12
	$\rightarrow 15/2_1^-$	0.1392	0.2235	100	100
1869	$19/2_1^- \rightarrow 17/2_1^-$	0.0559	0.3412	–	0.9
	$\rightarrow 15/2_2^-$	0.0034	–	–	0.02
	$\rightarrow 15/2_1^-$	0.1130	–	100	100
2248	$19/2_2^- \rightarrow 19/2_1^-$	0.0464	0.0111	–	11
	$\rightarrow 17/2_1^-$	0.1155	0.1821	48	260
	$\rightarrow 15/2_2^-$	0.0865	–	100	100
	$\rightarrow 15/2_1^-$	0.0042	–	45	91
2670	$21/2_1^- \rightarrow 19/2_2^-$	0.0288	0.2435	–	16
	$\rightarrow 19/2_1^-$	0.0872	0.1826	100	100
	$\rightarrow 17/2_1^-$	0.1485	–	70	51
2819	$23/2_1^- \rightarrow 21/2_1^-$	0.0480	0.4117	–	2
	$\rightarrow 19/2_2^-$	0.0083	–	–	0.5
	$\rightarrow 19/2_1^-$	0.1423	–	100	100
3253	$23/2_2^- \rightarrow 23/2_1^-$	0.0443	0.00005	159	2
	$\rightarrow 21/2_1^-$	0.0489	0.0985	100	100
	$\rightarrow 19/2_2^-$	0.1122	–	110	365
	$\rightarrow 19/2_1^-$	0.0012	–	136	19
3325	$25/2_1^- \rightarrow 23/2_2^-$	0.0233	0.1734	430	0.4
	$\rightarrow 23/2_1^-$	0.0528	0.1315	100	100
	$\rightarrow 21/2_1^-$	0.1626	–	10	74
3443	$27/2_1^- \rightarrow 25/2_1^-$	0.0001	0.00000001	1380	0.03
	$\rightarrow 23/2_2^-$	0.0002	–	–	0.5
	$\rightarrow 23/2_1^-$	0.0001	–	100	100
3708	$29/2_1^- \rightarrow 27/2_1^-$	0.1458	0.4246	100	100
	$\rightarrow 25/2_1^-$	0.0002	–	4	0.01
4045	$31/2_1^- \rightarrow 29/2_1^-$	0.0125	0.1592	100	100
	$\rightarrow 27/2_1^-$	0.0319	–	29	28
4454	$33/2_1^- \rightarrow 31/2_1^-$	0.0931	0.2699	100	100
	$\rightarrow 29/2_1^-$	0.0413	–	36	34
4927	$35/2_1^- \rightarrow 33/2_1^-$	0.0202	0.3138	100	100
	$\rightarrow 31/2_1^-$	0.0595	–	71	66
5440	$37/2_1^- \rightarrow 35/2_1^-$	0.0593	0.1721	100	100
	$\rightarrow 33/2_1^-$	0.0675	–	68	176
5933	$39/2_1^- \rightarrow 37/2_1^-$	0.0236	0.4559	44	98
	$\rightarrow 35/2_1^-$	0.0783	–	100	100
6501	$41/2_1^- \rightarrow 39/2_1^-$	0.0370	0.1093	80	29
	$\rightarrow 37/2_1^-$	0.0786	–	100	100

$N=77$ and even-even $N=78$ nuclei, respectively. We associate therefore the structure built on the $19/2^+$ level at 2197 keV in ^{139}Sm (labeled 5 in Fig. 2) to a $\nu s_{1/2}$ $(d_{3/2})$ $\otimes[\nu h_{11/2}]^2$ three-quasineutron configuration. In the core nucleus ^{140}Sm the analogous structure built on the 5^- state extends up to spin 11^- [45]. Calculations based on the interacting boson model with broken pairs have been performed for ^{140}Sm [34], with the fermion space containing the $h_{11/2}$ and the $d_{3/2}$ neutron orbitals. The calculated excitation energies for the negative-parity states are in agreement with ex-

perimental data. As pointed out in the previous subsection, the calculation of the corresponding states in ^{139}Sm requires the three-fermion positive-parity bases which are still prohibitively large. Nevertheless, we believe that, as in the case of ^{140}Sm, the IBM approach with broken pairs would give a satisfactory explanation for the positive-parity states discussed here.

C. The $\nu i_{13/2}$ highly-deformed band

Band 1 shows the most regular behavior. It consists of a cascade of $E2$ transitions and is interpreted as being built on the $\nu i_{13/2}$ intruder orbital [10,11], which of course is outside the model space used in the IBFM plus broken-pair calculations. The $I^{\pi} = 21/2^{+}$ spin-parity assignment to the bandhead, even if at variance with the $17/2^{+}$ one proposed in Ref. [10], is in accordance with the favored signature $[(\pi,\alpha)=(+,+1/2)]$ of the $\nu i_{13/2}$ orbital. Apart from the spin assignment here we are observing the same band as in the Stony Brook experiment [10]. We will not repeat therefore all the arguments of Ref. [10] (decay pattern, enhanced dynamical moment of inertia, aligned spins) in order to assign the $\nu i_{13/2}$ configuration to this particular band. We will only discuss what is really new with respect to the previous work, namely, the deformation which has been derived from the present measured lifetimes.

As stated in Sec. IV, a quadrupole moment $Q_0 = 3.9(7)$ eb has been extracted from the DSAM analysis of several transitions in the band. This value is smaller than that measured for bands of similar structure in the $A = 130-140$ region [5,12,13], being similar only to that derived for the HD band of the isotone ^{137}Nd, $Q_0 = 4.0(5)$ eb [14]. In this last case, under the assumption of an axially symmetric shape, a deformation parameter $\beta_2 = 0.22$ was obtained which is the smallest among the known HD or SD bands in the $A = 130$ mass region. If the same assumption is made for ^{139}Sm, a similar β_2 is derived. As the transition quadrupole moment is proportional to $\beta_2\cos(\gamma+30°)$, it has been pointed out [14] that the experimental result for ^{137}Nd is also compatible with a higher β_2 deformation if triaxiality is taken into account. Total Routhian surface calculations predict indeed a triaxial minimum ($\beta_2 = 0.27$, $\gamma \sim 10°-20°$) for the $\nu i_{13/2}$ configuration in ^{137}Nd [14]. The same calculations performed for ^{139}Sm [10] give a minimum at $\beta_2 = 0.27$ and $\gamma \sim 21°$ for the $\nu i_{13/2}$ configuration. Such deformation parameters are consistent with the experimentally determined quadrupole moment for the HD band in ^{139}Sm. The present data, together with those of ^{137}Nd, indicate a decrease in the quadrupole deformation and a larger triaxiality for the HD bands in the $A = 130-140$ mass region when moving from the Ce-Nd nuclei towards higher proton and neutron numbers. At the same time the bands become less regular [10,46] and show, as in the case of ^{139}Sm, strong variations of the dynamical moment of inertia caused by band crossings. According to cranked shell model calculations, such pronounced band crossings, almost absent in the $N = 75$ isotones, can be accounted for by the observed decrease of the quadrupole deformation, which results in a smaller interaction strength for quasiparticle pair alignment [10].

VI. CONCLUSIONS

A rich level structure has been established in the transitional nucleus ^{139}Sm by using the ^{110}Pd(^{34}S,$5n$) reaction. A band built on the $N = 6$ $\nu i_{13/2}$ intruder orbital has been identified and firmly connected to the lower-lying states. Furthermore, the quadrupole moment of the band has been measured, confirming its highly deformed character.

The main part of the remaining level structure has been discussed in the framework of the interacting boson-fermion model extended by the inclusion of a broken pair. In particular, good agreement is found between calculations and experiment for the high-spin negative-parity states, as well as for low-lying states of positive parity. The regular negative-parity sequence built on the $27/2^{-}$ state and dominated by strong $M1$ transitions is interpreted as a three-$h_{11/2}$ neutron configuration. The IBFM plus broken-pair description presents an alternative approach to the structure of regular $\Delta I = 1$ $M1$ bands recently observed in the $A = 130$ region, and which have been mainly discussed in terms of the tilted axis cranked shell model [47].

ACKNOWLEDGMENTS

We would like to acknowledge the valuable technical assistance of A. Buscemi, R. Isocrate, and R. Zanon in setting up the experiments. Thanks are due also to the staff of the XTU Tandem of LNL for the smooth operation of the accelerator.

[1] R. Bengtsson and S. Frauendorf, Nucl. Phys. **A314**, 27 (1979); **A327**, 139 (1979).
[2] W. Nazarewicz, R. Wyss, and A. Johnsson, Nucl. Phys. **A503**, 285 (1989).
[3] A. Atac, M. Piiparinen, B. Herskind, J. Nyberg, G. Sletten, G. de Angelis, R. M. Clark, S. A. Forbes, N. Giorup, G. B. Hagemann, F. Imbretsen, H. J. Jensen, D. Jerrestam, H. Kusakari, R. M. Lieder, G. V. Marti, S. Mullins, P. J. Nolan, E. S. Paul, P. H. Regan, D. Santonocito, H. Schnare, K. Strahle, M. Sugawara, P. O. Tjom, A. Virtanen, and R. Wadsworth, Phys. Rev. Lett. **70**, 1069 (1993).
[4] S. Lunardi, D. Bazzacco, C. Rossi Alvarez, P. Pavan, G. de Angelis, D. De Acuna, M. De Poli, G. Maron, J. Rico, O. Stuch, D. Weil, S. Utzelmann, P. Hoernes, W. Satula, and R. Wyss, Phys. Rev. Lett. **72**, 1427 (1994).
[5] P. J. Nolan, Nucl. Phys. **A553**, 107c (1993).
[6] F. Iachello and O. Scholten, Phys. Rev. Lett. **43**, 679 (1979).
[7] F. Iachello and D. Vretenar, Phys. Rev. C **43**, 945 (1991).
[8] D. Vretenar, G. Bonsignori, and M. Savoia, Z. Phys. A **351**, 289 (1995).
[9] D. Bazzacco, S. Lunardi, G. Nardelli, M. De Poli, and G. de Angelis, Z. Phys. A **335**, 363 (1990).
[10] P. Vaska, S. Bhattacharjee, D. B. Fossan, D. R. LaFosse, Y. Liang, H. Schnare, K. Starosta, M. P. Waring, I. Hibbert, R. Wadsworth, K. Hauschild, C. W. Beausang, S. Clarke, S. A. Forbes, P. J. Nolan, E. S. Paul, A. T. Semple, S. M. Mullins,

H. Grawe, and K. H. Maier, Phys. Rev. C **50**, 104 (1994).
[11] C. Rossi Alvarez, D. Bazzacco, S. Lunardi, N. Medina, R. Menegazzo, R. Venturelli, G. de Angelis, M. De Poli, D. R. Napoli, C. M. Petrache, D. Bucurescu, and C. Ur, Acta Phys. Pol. B **26**, 237 (1995).
[12] P. H. Regan, R. Wadsworth, S. M. Mullins, J. Nyberg, A. Atac, S. A. Forbes, D. B. Fossan, Y.-J. He, J. R. Hughes, I. Jenkins, R. Ma, M. S. Metcalfe, P. J. Nolan, E. S. Paul, R. J. Poynter, D. Santonocito, A. Virtanen, and N. Xu, J. Phys. G **18**, 847 (1992).
[13] E. S. Paul, S. A. Forbes, D. B. Fossan, J. Gizon, J. R. Hughes, S. M. Mullins, M. S. Metcalfe, P. J. Nolan, R. J. Poynter, P. H. Regan, G. Smith, and R. Wadsworth, J. Phys. G **18**, 121 (1992).
[14] S. M. Mullins, I. Jenkins, Y.-J. He, A. J. Kirwan, P. J. Nolan, J. R. Hughes, R. Wadsworth, and R. A. Wyss, Phys. Rev. C **45**, 2683 (1992).
[15] D. Bazzacco, in Proceedings of the International Conference on Nuclear Structure at High Angular Momentum, Ottawa, 1992 [Report No. AECL 10613 (unpublished)], Vol. 2, p. 376.
[16] J. Deslauriers, S. Gujrathi, S. K. Mark, and S. P. Sud, Z. Phys. A **325**, 421 (1986).
[17] L. K. Peker, Nucl. Data Sheets **59**, 767 (1990).
[18] A. Kerek, A. Luukko, M. Grecescu, and J. Sztarkier, Nucl. Phys. **A172**, 603 (1971).
[19] J. Gizon, A. Gizon, and D. J. Horen, Nucl. Phys. **A252**, 509 (1975).
[20] R. Ma, E. S. Paul, D. B. Fossan, Y. Lyang, N. Xu, R. Wadsworth, I. Jenkins, and P. J. Nolan, Phys. Rev. C **41**, 2624 (1990).
[21] J. Gizon, A. Gizon, M. R. Maier, R. M. Diamond, and F. S. Stephens, Nucl. Phys. **A222**, 557 (1974).
[22] J. Gascon, C.-H. Yu, G. B. Hagemann, M. C. Carpenter, J. M. Espino, Y. Iwata, T. Komatsubara, J. Nyberg, S. Ogaza, G. Sletten, P. O. Tjom, and D. C. Radford, Nucl. Phys. **A513**, 344 (1990).
[23] J. F. Ziegler, *Handbook of Stopping Cross Sections for Energetic Ions in All Elements* (Pergamon, New York, 1980).
[24] F. Iachello and A. Arima, *The Interacting Boson Model* (Cambridge University Press, Cambridge, 1987).
[25] F. Iachello and P. Van Isacker, *The Interacting Boson-Fermion Model* (Cambridge University Press, Cambridge, 1991).
[26] A. Arima and F. Iachello, Phys. Rev. Lett. **35**, 10 (1975).
[27] D. Vretenar, V. Paar, G. Bonsignori, and M. Savoia, Phys. Rev. C **42**, 993 (1990).
[28] D. Vretenar, V. Paar, G. Bonsignori, and M. Savoia, Phys. Rev. C **44**, 223 (1991).
[29] P. Chowdhury, C. J. Lister, D. Vretenar, Ch. Winter, V. P. Janzen, H. R. Andrews, D. J. Blumenthal, B. Crowell, T. Drake, P. J. Ennis, A. Galindo-Uribarri, D. Horn, J. K. Johansson, A. Omar, S. Pilotte, D. Prevost, D. Radford, J. C. Waddington, and D. Ward, Phys. Rev. Lett. **67**, 2950 (1991).
[30] D. Vretenar, G. Bonsignori, and M. Savoia, Phys. Rev. C **47**, 2019 (1993).
[31] C. J. Lister, P. Chowdhury, and D. Vretenar, Nucl. Phys. **A557**, 361c (1993).
[32] A. A. Chisthi, P. Chowdhury, D. J. Blumenthal, P. J. Ennis, C. J. Lister, Ch. Winter, D. Vretenar, G. Bonsignori, and M. Savoia, Phys. Rev. C **48**, 2607 (1993).
[33] G. de Angelis, M. A. Cardona, M. De Poli, S. Lunardi, D. Bazzacco, F. Brandolini, D. Vretenar, G. Bonsignori, M. Savoia, and R. Wyss, Phys. Rev. C **49**, 2990 (1994).
[34] R. Menegazzo, Y. Li, S. Lunardi, G. de Angelis, D. Bazzacco, C. Rossi Alvarez, F. Brandolini, M. De Poli, and D. Vretenar, Legnaro Annual Report LNL-INFN (Rep)-095/95, 1994, p. 38.
[35] D. Bazzacco, F. Brandolini, K. Löwenich, S. Lunardi, P. Pavan, C. Rossi Alvarez, F. Soramel, M. De Poli, A. M. I. Haque, and G. de Angelis, Phys. Lett. B **206**, 404 (1988).
[36] V. A. Bondarenko, I. L. Kuvaga, P. T. Prokofjev, V. A. Khitrov, Yu. V. Kholnov, Le Hong Khiem, Yu. P. Popov, A. M. Sukhovoj, S. Brant, V. Paar, and V. Lopac, Nucl. Phys. **A551**, 54 (1993).
[37] R. E. Chrien, B. K. S. Koene, M. L. Stelts, R. A. Meyer, S. Brant, V. Paar, and V. Lopac, Phys. Rev. C **48**, 109 (1993).
[38] V. A. Bondarenko, I. L. Kuvaga, P. T. Prokofjev, A. M. Sukhovoj, V. A. Khitrov, Yu. P. Popov, S. Brant, and V. Paar, Nucl. Phys. **A582**, 1 (1995).
[39] R. E. Chrien *et al.* (unpublished).
[40] L. S. Kisslinger and R. A. Sorensen, Rev. Mod. Phys. **35**, 853 (1963).
[41] S. Brant *et al.* (unpublished).
[42] D. Bucurescu, D. Barnéoud, Gh. Cata-Danil, T. von Egidy, J. Genevey, A. Gizon, J. Gizon, C. F. Liang, P. Paris, B. Weiss, S. Brant, V. Paar, and R. Pezer, Nucl. Phys. **A587**, 475 (1995).
[43] B. S. Reehal and R. A. Sorensen, Phys. Rev. C **2**, 819 (1970).
[44] A. Zemel, C. Broude, E. Dafni, A. Gelberg, M. B. Goldberg, J. Gerber, G. J. Kumbartzki, and K. H. Speidel, Z. Phys. A **304**, 269 (1982).
[45] S. Lunardi, D. Bazzacco, G. Nardelli, F. Soramel, J. Rico, E. Maglione, M. De Poli, and G. de Angelis, Phys. Rev. C **42**, 174 (1990).
[46] S. M. Mullins, A. Omar, L. Persson, D. Prevost, J. C. Waddington, H. R. Andrews, G. C. Ball, A. Galindo-Uribarri, V. P. Janzen, D. C. Radford, D. Ward, T. E. Drake, D. B. Fossan, D. R. LaFosse, P. Vaska, M. P. Waring, and R. Wadsworth, Phys. Rev. C **47**, R2447 (1993).
[47] S. Frauendorf, Nucl. Phys. **A557**, 259c (1993).